Depinning regimes and contact angle hysteresis of a drop on doubly periodic microtextured surfaces

Stanimir Iliev[*] and Nina Pesheva[†]
Institute of Mechanics, Bulgarian Academy of Sciences, Acad. G. Bonchev St. 4, 1113 Sofia, Bulgaria

Pavel Iliev[‡]
ETH Zurich, Computational Physics for Engineering Materials, CH-8093 Zurich, Switzerland

(Received 3 February 2020; accepted 14 April 2020; published 11 May 2020)

We investigate numerically the drop shape evolution under quasistatic drop volume change on doubly periodic microtextured surfaces in the framework of the capillary model. Taking into account the symmetries of the periodic lattice of defects, we study the drop contact line (CL) motion along all lines of symmetry, allowing us to get a more complete view of the CL behavior. Four CL depinning regimes for a liquid drop are distinguished related to the stick, slip, and jump motion of the CL. The distinction of the different regimes is made based on the region of the CL where the process starts and on whether the start of the depinning is related to detaching from a defect or to the CL reaching a new row of defects. For every type of depinning regime we study the advancing and receding apparent contact angles (CAs) as functions of the defect concentration. We established a relation between the results for the CL depinning and the CA hysteresis (CAH) for a drop on hydrophilic and hydrophobic heterogeneous surfaces. A comparison of the obtained numerical results for the CAH is made with the existing theoretical, experimental, and numerical data.

DOI: 10.1103/PhysRevE.101.052801

I. INTRODUCTION

The understanding of the contact characteristics of a liquid drop placed on doubly periodic microtextured surfaces has made significant progress during recent years [1–3]. The related studies are motivated by the desire of obtaining solid surfaces on which the drop starts rolling at low surface inclination angles. These surfaces are characterized by a small contact angle (CA) hysteresis (CAH). The latter is defined as the difference between the advancing contact angle (ACA) and the receding contact angle (RCA). Since the determination of the CAH of a drop in contact with a rough surface, covered with physical defects such as posts or holes, can be reduced in most cases to the simplified problem of obtaining the CAH on a smooth surface with chemical defects [4,5], investigations of drops in contact with chemically heterogeneous surfaces have intensified and advanced significantly in recent years. The experimental studies are most often conducted on surfaces with periodically distributed defects, due to which the theoretical analysis of CAH is also directed predominantly to this case. For the latter case, the mechanism of a drop's contact line (CL) displacements (comprising slip, jump, and stick motion) is studied. The result of this displacement is that when the CL is in contact with one row of defects, it moves as a whole to form a contact with the neighboring row of defects, overcoming the pinning due to the elastic force [6]. The most studied case is that of a periodic CL whose period equals the distance between the centers of two neighboring defects [5,7–14]. In this situation, the whole CL moves from a contact with one row of defects to the next row, and this is called *block case* [15] depinning. This behavior of the CL is pertinent to the situation when a liquid in a vessel is in contact with a partially immersed solid plate [16]. However, it is questionable whether it is applicable to a liquid drop whose CL forms a closed contour. For the RCA of a liquid drop on a rough solid surface with posts, Raj *et al.* [12] report the results of an experiment, supporting the prediction of a block case depinning, while Dorrer and Rühe [17] and Gauthier *et al.* [18] report that they observe a deviation from this case experimentally. According to the latter authors, the reason for the deviation of the RCA from the prediction of the block case in the context of a drop geometry is that another depinning regime, termed kink case [15] depinning, is taking place. In this regime, the receding CL (RCL) passes from one row of defects to another row through series of single jumps (or depinnings) from one defect at a time, starting in regions where the equilibrium CL crosses from one row of defects to the next. Such transitions of the CL are observed experimentally [18]. Moreover, a series of successive single jumps, when passing from one row of defects to another, is observed experimentally also for an advancing CL (ACL) in the case when a liquid drop is placed on a flat surface with chemical defects [19]. In contrast to the RCL case, in the advancing regime the depinning starts at the middle section of the CL, which is in contact with one row of defects.

The availability of alternative approaches for determining the CAH, arising due to different scenarios and regimes of CL depinning, makes it feasible to get a more complete and precise understanding of the appearance of the CAH by

[*]stani@imbm.bas.bg
[†]nina@imbm.bas.bg
[‡]ilievp@ethz.ch

explicitly analyzing the stick, slip, and jump motion of the ACL and RCL for different physicochemical characteristics of the defects. In this way, one can find out precisely which depinning regime is responsible for the appearance and the value of the CAH in every specific situation.

It is clear that in the case of a drop, the whole CL cannot pass simultaneously from one row of defects to another. However, for the determination of the CAH it is of interest to know whether the predictions of the block depinning case or the kink depinning case are applicable for the particular situation under consideration. The above cited experimental and analytical results do not give a clear indication of that. Finding a solution to this problem requires one to study more thoroughly and analyze the stick, slip, and jump motion of the drop's ACL and RCL for different possible realizations of the physicochemical characteristics of the defects.

Taking into account the complexity of this problem, one needs to perform numerical simulations of the behavior of a drop on microtextured surfaces. Until now, only an isolated solution for the RCL and the RCA has been obtained numerically [20] (by the help of the SURFACE EVOLVER software package) within the framework of the classical capillary theory. The series of ACLs and RCLs, which appear when a small quasistatic change of the drop volume is made, are obtained by application of the lattice Boltzmann algorithm [21] and by means of phase field theory [22]. In these studies, however, an analysis of the depinning mechanisms of the CL and also the appearance and the value of the CAH, which are related to the depinning mechanisms, was not performed. Parametric analysis of the kink case depinning was done numerically only for a RCA in the Wilhelmy plate geometry [5,15,18]. However, the use of these results for the analysis of the kink case depinning mechanism for a drop's CL is questionable, since in the case of the Wilhelmy plate geometry the elastic force is acting to straighten the CL, while in the case of a drop placed on a surface it is trying to lend it a circular form [17].

The main goal of the present work is to study these processes by investigating the evolution of the CL of numerically obtained equilibrium drop shapes within the framework of the classical capillary model under varying (increasing or decreasing) drop volume. We focus on the most studied case when the drop is in contact with a heterogeneous solid surface covered with regularly spaced circular defects, forming a rectangular lattice. The CL depinning is investigated for both ACL and RCL. We also consider the cases of a drop in contact with hydrophilic and hydrophobic heterogeneous solid surfaces.

II. PROBLEM DESCRIPTION

We consider a small three-dimensional (3D) equilibrium liquid drop with volume V and free surface Σ, placed on a flat, well-structured two-component chemically heterogeneous solid plate Σ_s, forming with it a CL $L = \Sigma \cap \Sigma_s$. The solid plate Σ_s is composed of circular "mesa"-type defects [6] with radius r, constituting a doubly periodic pattern denoted by Σ_s^d, and the homogeneous base, Σ_s^b (the superscripts d and b stand for defect and base, respectively). The rectangular lattice of circular defects has spatial periods $\lambda_1 \geqslant \lambda_2$, $\lambda_2 \gg r$. The two materials, Σ_s^d and Σ_s^b, are characterized by their local equilibrium CAs θ^d and θ^b, respectively, which the liquid forms with the two surfaces.

Since gravity does not significantly influence the problems under study here, we consider the case where the equilibrium drop shape is formed solely by the balance of surface tensions. In this case the metastable equilibrium drop shapes are obtained through minimization of the functional [23] $U(\Sigma)$ at fixed drop volume $V = V(\Sigma)$,

$$U(\Sigma) = S(\Sigma) - \cos\theta^d S^d(\Sigma) - \cos\theta^b S^b(\Sigma), \qquad (1)$$

where S, S^d, and S^b are the liquid-air and the solid-liquid interface areas in contact with Σ_s^d and with Σ_s^b, respectively.

We obtain numerically a sequence of equilibrium drop shapes, $\Sigma_0, \Sigma_1, \Sigma_2, \ldots$, for different drop volumes, $V_0, V_1, V_2, \ldots; V_{i+1} = V_i \pm \Delta V$, $(\Delta V \ll V)$, where ΔV is the drop volume change. For the initial volume $V = V_0$, we obtain the equilibrium drop shape Σ_0, starting with the spherical cap approximation of the drop shape with circular CL, having radius R and forming with the solid plate Σ_s a CA, equal to the Cassie's angle θ^C, on the two-component surface,

$$\theta^C = \cos^{-1}(p\ \cos\theta^d + (1-p)\ \cos\theta^b), \qquad (2)$$

where p is the defect surface concentration. Every next equilibrium drop shape, Σ_i, we obtain in the following two-step process. First, we slightly deform the drop shape Σ_{i-1}, but keeping the drop's CL unchanged so that the drop volume V (encompassed between the drop surface Σ and the solid plate Σ_s) is increased or decreased by a small amount ΔV. Second, starting with the so-obtained free surface, we apply the numerical algorithm for minimization of the functional, U [Eq. (1)], for the class of deformations which keep the drop's volume unchanged. The free surface obtained in this way is the required equilibrium drop surface Σ_i corresponding to drop volume V_i.

The obtained results will be shown in the dimensionless Cartesian coordinate system $x/\lambda_2, y/\lambda_2, z/\lambda_2$, where the plane $z = 0$ coincides with the heterogeneous solid surface on which the drop is placed, and the center of the drop's CL coincides with the origin of the coordinate system. We assume that in this system the defect centers are positioned on a rectangular lattice with lines which are parallel to x and y axes with spatial periods 1 and λ_1/λ_2, respectively. The so-defined two-component chemically heterogeneous surface is characterized by several planes of symmetry. Planes of symmetry are found at angles $\varphi = 0^\circ$, $\tan^{-1}(\lambda_2/\lambda_1)$, 90° with respect to the principal lattice axes. Thus rows of defects exist along all these directions, however, characterized by different periods.

We are interested in determining the biggest (maximal) and the smallest (minimal) CAs related to the local CL motion as the drop recedes or advances across the rows of defects along all of the above symmetry directions. For this purpose, we calculate the CA on the macroscopic scale as defined in Ref. [24] (termed apparent CA) along all directions of symmetry of the defect lattice by using a modification of the standard projection method [25].

To calculate this angle, we use a fit of the drop profile, obtained in the side view of the drop (see Fig. 1). For the fitting we use only points from the drop's profile up to a distance from the three-phase point bigger than the spread l_s along

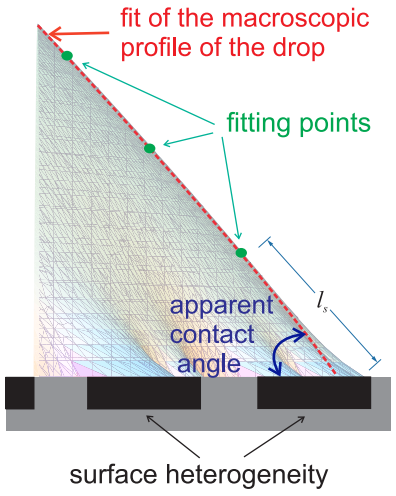

FIG. 1. Schematic of the drop edge deformation, drop projection profile fitting, and the apparent contact angle.

the drop-free surface of the perturbation of the CL, caused by the presence of periodic defects on the solid surface. Previous studies [26,27] estimate that distance l_s to be of the order of the defect's lattice period.

We numerically obtain the equilibrium drop shape through a minimization of the functional, Eq. (1), by applying a numerical algorithm developed earlier [28]. The method and the numerical algorithm are similar to those used in the public domain software SURFACE EVOLVER [29]. Our numerical algorithm was used previously for the study of a drop on heterogeneous substrates, having radial symmetry, and also for the dart board substrate [30]. In Ref. [23] it is shown that the obtained solution for the equilibrium drop shape on heterogeneous surfaces through the minimization algorithm mentioned above satisfies the Laplace equation for the equilibrium drop shape with high precision. In the present study, the approximation of the drop surface, Σ, has a significantly larger fixed number of nodes—approximately $N > 103\,000$—and the CL is approximated by 1080 line segments. The approximation of the drop surface Σ in the neighborhood of the CL is shown in Fig. 9(b) below.

III. NUMERICAL RESULTS AND DISCUSSION

For a more complete and in-depth study of the CL depinning mechanisms and CAH in the drop geometry, we perform numerical simulation and analysis of the drop shape evolution on both *hydrophilic and hydrophobic heterogeneous surfaces*. In addition, we also differentiate the cases when $\theta^d < \theta^b$ and $\theta^d > \theta^b$ for both types of surfaces. Thus to get the whole picture one needs to study the evolution of the drop shape in four distinct cases when the drop volume is increasing and similarly, in four cases when the drop volume is decreasing.

A. Hydrophilic surfaces

As a representative case for the hydrophilic surfaces we choose the values of 30° and 80° for the pair of angles $\{\theta^d,\ \theta^b\}$. Numerical simulations performed for different values of these angles show that the results obtained for the pair $\{30°, 80°\}$ reflect the typical behaviors of the CL, RCA, and ACA for a drop on hydrophilic surfaces. We start the numerical study with a spherical cap approximation of the drop with circular CL with radius $R = 14$. This choice of drop radius value allows one to study a drop CL, which passes through a sufficiently large number of defects, ranging up to 80. Drop shape solutions are obtained also for different values of the defects radius r so that the surface defect concentration, defined by $p = \pi r^2/(\lambda_1\lambda_2)$, varies in the interval $0.1 \leqslant p \leqslant 0.55$ and different values of the ratio of the lattice spatial periods $\lambda_2/\lambda_1 \in [1, 3]$.

1. Depinning regimes

The analysis of the numerical solutions for the CL evolution under volume increase, obtained for different values of the surface defect concentration p and different values of the ratio λ_2/λ_1, show that one can distinguish *four types of depinning regimes* (summarized below in Table I) when the CL moves from one row of defects to another. The types of depinning regimes do not depend on these parameters (p and λ_2/λ_1); however, they depend on whether the CL is advancing or receding and also on whether $\theta^d < \theta^b$ or $\theta^d > \theta^b$. They are the same for all displacements of the CL along the directions defined by the angles $\varphi = 0°, \tan^{-1}(\lambda_2/\lambda_1), 90°$. These depinning regimes are illustrated in Figs. 2–5 for defects located on a square grid ($\lambda_2 = \lambda_1$) with defect concentration $p = 0.4$, and also for both increasing and decreasing drop volume cases. In the (a) panels of Figs. 2–5, parts of the CLs are shown where one can observe the behavior of the CL displacements along the 0° and 45° directions. Part of these CLs are shown on a larger scale in the respective (b) panels of Figs. 2–5, where one can observe the CL in more detail, moving along the 0° direction. The equilibrium CL L_0, obtained at the start of the minimization algorithm using the spherical cap approximation of the drop shape, is shown in the figures with dotted (black) lines. The equilibrium CLs immediately preceding the process of transition of the CL to the next row of defects, and the resulting CLs after the depinning, along directions $\varphi = 0°$ and 45°, are shown by bold and thin solid (blue) and dash-dotted (red) lines, respectively. In

TABLE I. Types of depinning regimes and their correlation with the stick-slip behavior of the contact line. The depinning case is determined based on the part of the CL where the process starts, and further distinction of the type of depinning is made by the way the depinning is started.

	ACL depinning			RCL depinning		
Hydrophilic surface	Case	Type	Label assigned	Case	Type	Label assigned
$\theta^d < \theta^b$	Block (***B***)	By reaching a defect (***R***)	***BR***	Kink (***K***)	By detaching from a defect (***D***)	***KD***
$\theta^d > \theta^b$	Block (***B***)	By detaching from a defect (***D***)	***BD***	Kink (***K***)	By reaching a defect (***R***)	***KR***

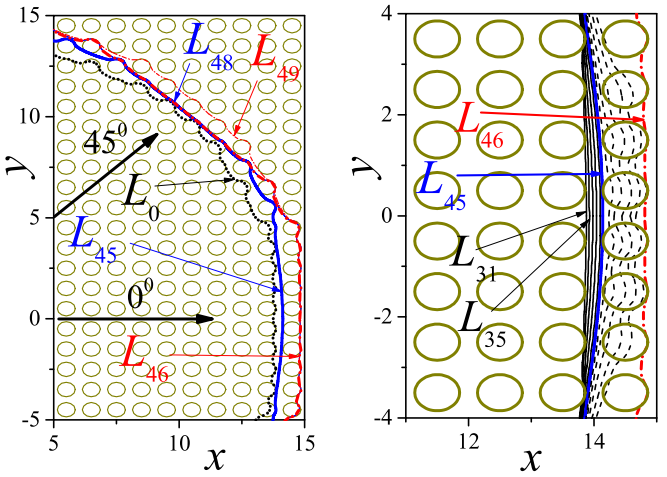

FIG. 2. (a) Parts of advancing CLs of a drop on heterogeneous surfaces when $\{\theta^d = 30^\circ,\ \theta^b = 80^\circ\}$ along directions $\varphi = 0^\circ, 45^\circ$. L_0 [short dashed (black) line] is the initial equilibrium CL; CLs L_{45} [bold (blue) line] and L_{48} [thin (blue) line] are the equilibrium CLs immediately preceding the process of transition of the CL to the next defect row along directions $\varphi = 0^\circ$ and 45°, respectively; CLs L_{46} [bold (red) dashed-dotted line] and L_{49} [thin (red) dashed-dotted line] are the resulting equilibrium CLs after the depinning. (b) Blown-up image of the region in (a) (in the lower right corner) where the CL detaches from one row of defects and moves to another along direction $\varphi = 0^\circ$. CLs L_{31}, L_{35} to L_{45} show few CLs from the sequence of equilibrium CLs (generated by drop volume increase ΔV) before the CL depinning; the dashed (black) lines illustrate some of the CLs in the sequence of the drop CL displacements (from left to right) during the transition from the equilibrium CL L_{45} towards equilibrium CL L_{46}, appearing during the minimization process of the energy Eq. (1).

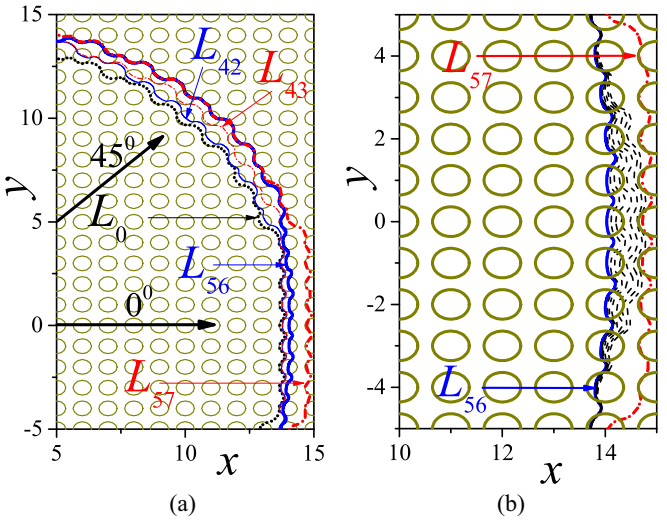

FIG. 3. Same as in Fig. 2, however, for a heterogeneous surface, characterized by $\{\theta^d = 80^\circ,\ \theta^b = 30^\circ\}$, i.e., when $\theta^d > \theta^b$. CLs L_{56} and L_{42} are the CLs just before the depinning in the $\varphi = 0^\circ$ and 45° directions, respectively; CLs L_{57} and L_{43} are the respective CLs after the depinning (the blue lines show the CLs before the depinning and the red lines after the depinning).

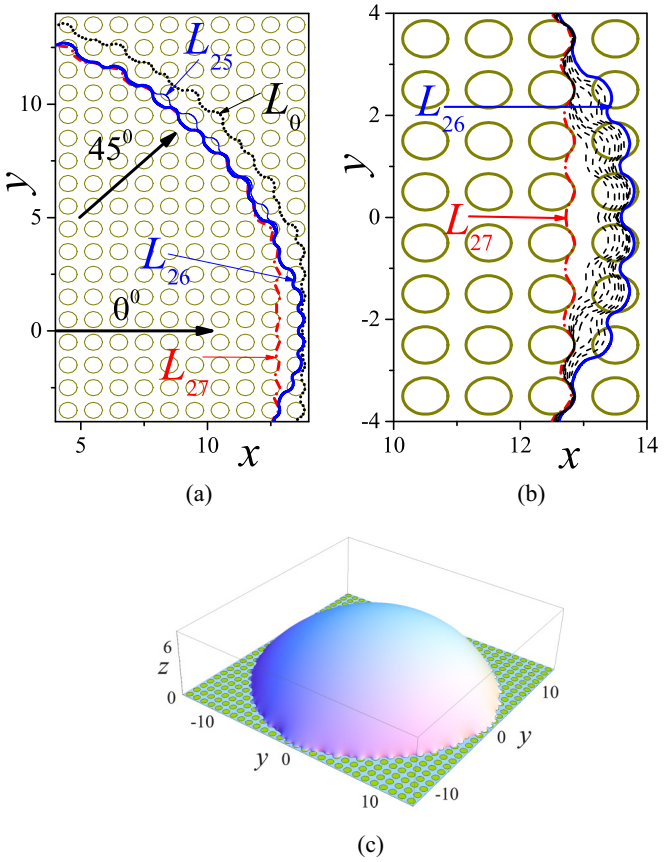

FIG. 4. (a) Parts of the obtained RCLs for a drop on a heterogeneous surface $\{\theta^d = 30^\circ,\ \theta^b = 80^\circ\}$. CLs L_{26} and L_{25} are the CLs just before the depinning in directions $\varphi = 0^\circ$ and 45°, respectively; CL L_{27} is the CL after the depinning. (b) Enlarged view of the RCLs displayed in (a) (in the lower right corner) showing the successive small displacements of the CL during the transition from the outer row of defects to the inner row along direction 0°. (c) General 3D view of the equilibrium drop with a CL L_{26} [shown also in parts (a) and (b)] just before the CL depinning occurs.

Figs. 2(b)–5(b) with thin dashed (black) lines are presented several intermediate (nonequilibrium) CLs which appear in the CL depinning process during the transition from one equilibrium drop state (which is driven out of equilibrium due to the change in drop volume) to a new equilibrium drop state. The analysis of the sequence of intermediate CLs appearing between the two successive equilibrium drop states during the minimization process shows that this sequence of CLs models well the quasistatic relaxation of the contact line [31] within the framework of the contact line dissipation approach (see [32] and [33]).

Advancing CL. Figures 2 and 3 present our results for the case of advancing CLs (i.e., when the sequence of the equilibrium CLs is generated by increasing the drop volume) when $\theta^d < \theta^b$ and when $\theta^d > \theta^b$, respectively. In this (advancing) case, each subsequent CL, equilibrium or intermediate, is either partially overlapping or enclosing the previous CL. The sequence of dashed lines in Figs. 2(b) and 3(b), ordered consecutively in a direction from the center to the outer part of the drop, illustrates the CL jump process from the inner to the outer row of defects in direction 0° (i.e., along the x axis).

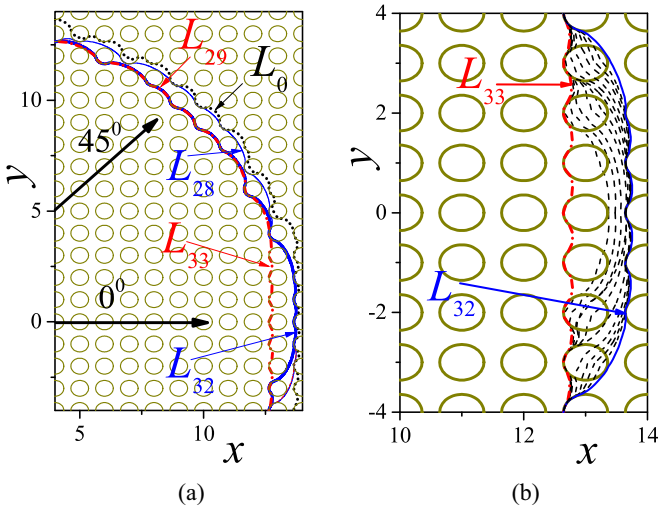

FIG. 5. (a) Parts of the obtained RCLs when $\{\theta^d = 80°,\ \theta^b = 30°\}$. CLs L_{32} and L_{28} are the CLs just before the depinning in directions $\varphi = 0°$ and 45°, respectively; CLs L_{33} and L_{29} are the respective CLs after the depinning. (b) Enlarged view of the CL detachment along direction 0° from part (a) showing the successive small displacements of the CL during the transition from one (outer) row of defects to another (inner) row of defects.

When $\theta^d < \theta^b$, it starts from the equilibrium CL L_{45} and goes to the equilibrium CL L_{46}, and when $\theta^d > \theta^b$ it is from L_{56} to L_{57}, respectively.

When $\theta^d < \theta^b$, as is seen in Fig. 2, the detachment of the CL from the inner row of defects and its adherence to an outer row of defects along direction $\varphi = 0°$ is not realized within a single small change ΔV in the drop volume. The simulations indicate that when the CL L_{30} is reached after 30 droplet volume increases ΔV, it transforms to the depicted section of the CL L_{31} [see Fig. 2(b)] of the new equilibrium drop state, whose middle section is positioned only on the base surface Σ_s^b without touching the defects located there. It can be observed that in the middle section of the CL, L_{31}, there is a detachment, which remains localized, i.e., it does not propagate to adjacent defects and does not jump to the outer row of defects. With the further increase in the drop volume, the detachment expands smoothly, with the CL forming a circular shape in the area, where it is detached from the defects, and it approaches the outer row of defects. This behavior is observed for the CLs between L_{31} and L_{45}. The jumping process starts when the detached part of the CL reaches the defect border belonging to the outer row of defects. In the case under consideration here, this is realized after the volume increase at CL L_{45}. Along the direction defined by 45°, the detachment of the CL from an inner row of defects and its adherence to an outer row is realized in a similar way; however, the detachment of the CL from the defects and the establishment of a contact with the outer row of defects is accomplished for smaller change of the drop volume (even for just one ΔV). The reason for this is that in this direction (as seen in Fig. 2, from L_{48} to L_{49}) the distance between the neighboring rows of defects is very small or even negative. The CL reaches an outer row of defects without the need to detach from a defect first.

When $\theta^d > \theta^b$, the case shown in Fig. 3, the detachment of the CL from the inner row of defects and its adherence to the outer row is realized within a single volume increase ΔV. This is valid for both considered directions (0° and 45°) as well as for different surface concentrations p. Along direction 0° [see Fig. 3(b)], the CL L_{56} detaches first from the row of defects (with centers on line $x = 14$), then the CL jumps to the next (outer) row of defects (with centers on the line $x = 15$), and adheres to them. This happens when the elastic force overcomes the stick force, which keeps the CL in contact with the inner part of the defects. As illustrated in Fig. 3(b) by the sequence of intermediate CLs, this process is realized as a series of consecutive detachments of the CL from the defects, starting from the central part ($y = 0$) of the CL.

In both cases ($\theta^d < \theta^b$ and $\theta^d > \theta^b$) the CL detachment starts from the middle section of the part of the CL which is in contact with one row of defects. The displacements of the CL along the considered directions are localized within one row of defects. Therefore, this category of depinning can be labeled as *block (B) case depinning*, but proceeding in two different ways. In one realization (when $\theta^d < \theta^b$), it is initiated by reaching (R) the border of a defect, belonging to a new row of defects, and we abbreviate it *BR-type depinning*. In the other realization (when $\theta^d > \theta^b$), it is initiated by detaching (D) from the inner part of a defect and we call it *BD-type depinning* (see Table I).

Receding CL. Figures 4 and 5 present our results for receding CLs, i.e., when the sequence of CLs is generated by decreasing the drop volume, when $\theta^d < \theta^b$ and $\theta^d > \theta^b$, respectively. In the receding case, each subsequent CL (equilibrium or intermediate) is partially overlapping with the previous CL or is inscribed in it. The numerically obtained 3D equilibrium drop shape is shown in Fig. 4(c) with a contact line L_{26}—just before the depinning of the CL in direction 0° occurs.

When $\theta^d < \theta^b$ ($\theta^d = 30°,\ \theta^b = 80°$), the case shown in Fig. 4, the transition of the CL to the internal row of defects along direction 0° occurs when the CL elastic force overcomes the pinning force, keeping the CL attached to the last defect (the defect with center at (13.5, 2.5), located on the row of defects with centers on the line $x = 13.5$. In Fig. 4(b) this precise moment occurs when a slight decrease in the volume of the droplet is made when the drop CL is L_{26}. As a result, in the vicinity of this defect, the CL jumps, reaching the defect with center at (12.5, 2.5) and forms a contact with it along part of its boundary. This causes the CL to move along the defect centered at (13.5, 1.5), related to an increase of the elastic force and a decrease of the pinning force in that region. The latter leads to the continuation of the cascading process of depinning—the end result being the new equilibrium CL L_{27}, which is not in contact with the row of defects with centers on the line $x = 13.5$. For the CL depinning along the 45° direction, one observes a specificity, as in the CL advancing regime, due again to the closeness of the rows of defects along the direction of the CL displacement. When decreasing the drop volume, the CL reaches the inner row of defects without detaching from the outer row of defects and a new CL is formed, positioned on two neighboring rows of defects. An example of such CL is the CL L_{25} shown in Fig. 4(a). With further decrease of the drop volume, this CL, again due to

overcoming of pinning force by the elastic force, jumps to the inner row of defects. At small surface defect concentrations this peculiarity is not observed and the CL depinning is similar to that appearing along direction 0°.

When $\theta^d > \theta^b$ ($\theta^d = 80°,\ \theta^b = 30°$), as can be seen from Fig. 5, the transition to the inner row of defects occurs when the CL reaches and makes contact with a defect from the inner row of defects due to the drop volume decrease, leading to a cascade of CL displacements. This process is identical along the two directions considered, 0° and 45°, and starts when the CL reaches a defect belonging to the inner row. This precise moment occurs in Fig. 5 when a slight decrease in the volume of the droplet is made when the drop CL is L_{32}—when the CL displacement along direction 0° and L_{28} along direction 45° are considered. As shown in Fig. 5(b), along direction 0° after the CL establishes a contact with the defect centered at (13,3), during the minimization of the functional U [see Eq. (1)] the nonequilibrium CL jumps to the other end of the defect. In the course of CL displacement, CL breaks away from the defect centered at (14,2), then touches the defect centered at (13,2), after which a similar process is repeated until the nonequilibrium CL is completely detached from the row of defects with centers on the line $x = 14$.

From Figs. 4 and 5, it can be seen that in the case of a receding CL, the depinning starts from the CL sections, where the equilibrium CL passes from one row of defects to another. In the receding mode, this situation gives grounds for the depinning to be designated as a *kink* (K) *case depinning*. But again, as in the case of advancing CL, two different depinning types are observed—one associated with a CL reaching (R) the border of a new defect from the neighboring row and making a contact with it and second one associated with a CL detaching (D) from a defect, respectively. We call the first realization a *KR-type depinning* and the second one a *KD-type depinning*, similarly to the situation in the block-case depinning (see also Table I).

Thus, the analysis of the CL depinnings for a drop, as illustrated in Figs. 2–5, gives grounds to distinguish *four depinning regimes*, presented in Table I. We find that the following relation holds between the advancing and receding modes on the same heterogeneous surface. If in advancing mode one has a BR-type depinning, then in the receding mode a KD-type depinning occurs, and vice versa, i.e., if in advancing mode a BD-type depinning is occurring, then a KR-type depinning takes place in receding mode.

The numerical studies for a *rectangular grid* of defects with $\lambda_1 > \lambda_2$, $\lambda_1 \leqslant 3$, show that the characteristics of the CL depinning regimes, obtained for square lattice, remain unchanged.

2. CAH

For a drop on the considered substrate, by utilizing the existing symmetries of the system, as a first approximation one can consider the CL displacements from one row of defects to the neighboring row along the lines of symmetry. The ACA and the RCA are the biggest (maximal) and the smallest (minimal) among the equilibrium CAs, which are formed between the drop surface and the substrate along the lines of symmetry. Through the ACA and RCA one can determine the CAH, defined as the difference between the two angles.

For a square lattice it is sufficient to determine the maximal and minimal apparent CAs along directions 0° and 45°, i.e., $\theta_0^{\max}, \theta_0^{\min}, \theta_{45}^{\max}, \theta_{45}^{\min}$, respectively. The ACA θ^a is the bigger angle of the pair $\theta_0^{\max}, \theta_{45}^{\max}$, i.e., $\theta^a = \max\{\theta_0^{\max}, \theta_{45}^{\max}\}$, and the RCA θ^r is the smaller angle of the pair $\{\theta_0^{\min}, \theta_{45}^{\min}\}$, i.e., $\theta^r = \min\{\theta_0^{\min}, \theta_{45}^{\min}\}$. These angles are obtained through the procedure (described in Sec. II) for determination of the apparent CA for equilibrium drop shapes, having CLs preceding the CL depinning along the respective direction (0° or 45°). The numerical studies indicate that when fitting the drop profile one has to consider points whose distance to the CL is greater than the distance between the defect centers λ_1. That can be seen also from the parts of the 3D shape of a droplet [shown in Figs. 4(c) and 9(b)] with a CL just before the depinning begins by finding the distance (from the CL along the drop profile) at which the local perturbation of the CL spreads. All results reported below are obtained in this way.

ACA. The obtained numerical results show that for the whole range of investigated defect concentrations $p \in [0.1,\ 0.55]$, the biggest CAs $\theta_0^{\max},\ \theta_{45}^{\max}$ for a drop coincide with the predictions [12] for ACA, made by the block depinning model of a CL, located on a single row of defects. For a substrate where the pair of CAs $\{\theta^d,\ \theta^b\}$ have values $\{30°, 80°\}$, the biggest CA coincides with the numerical results [13] for the ACA in the Wilhelmy plate geometry.

In the case where the CL depinning is initiated by CL making a contact with a new defect (when $\theta^d < \theta^b$), the ACA $\bar{\theta}^a$, as predicted by the block depinning model, is equal to the angle characterizing the homogeneous base Σ_s^b, i.e.,

$$\bar{\theta}^a = \theta^b. \tag{3}$$

Thus one has $\theta_0^{\max}, \theta_{45}^{\max} = \bar{\theta}^a = \theta^b$. The reason for this result, appearing in direction 0°, is the observation made above for the evolution of the CL [shown in Fig. 2(b)], that before the CL reaches a defect from the outer row, much of it is already detached from the inner row of defects. Due to the fact that in a large area the CL is in contact only with the base surface with local CA θ^b, it follows that in the central point in this area the apparent CA is the same. These observations and reasoning hold true also when considering the CL displacements along the 45° direction, where almost the entire CL is positioned on the base surface.

In the case where the CL depinning is triggered by a detachment from a defect (when $\theta^d > \theta^b$), according to the predictions of the block depinning model, the ACA $\bar{\theta}^a$ is determined by the linearized Cassie equation [7,12,17],

$$\cos\bar{\theta}^a = p_l \cos\theta^d + (1 - p_l)\cos\theta^b, \tag{4}$$

where p_l is the linear fraction [34] of the contact line that resides on the defects, i.e.,

$$\cos\theta_0^{\max} = \frac{2r}{\lambda_2}\cos\theta^d + \left(1 - \frac{2r}{\lambda_2}\right)\cos\theta^b;$$
$$\cos\theta_{45}^{\max} = \frac{2r}{\sqrt{2}\lambda_2}\cos\theta^d + \left(1 - \frac{2r}{\sqrt{2}\lambda_2}\right)\cos\theta^b. \tag{5}$$

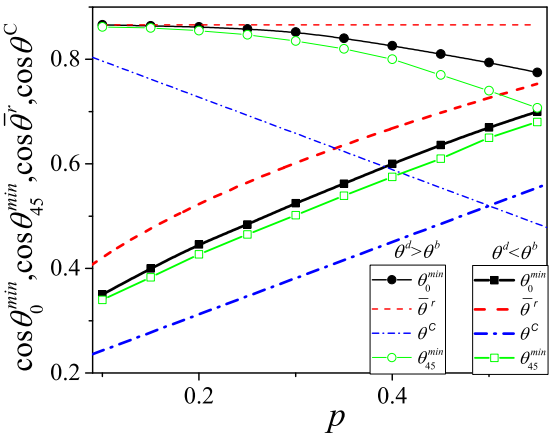

FIG. 6. The cosines of the smallest CAs, $\theta_0^{\min}$ and $\theta_{45}^{\min}$, $\bar{\theta}^r$ [Eqs. (6) and (7)], and Cassie's angles θ^C as functions of the defect surface concentration p when $\theta^d < \theta^b$ and when $\theta^d > \theta^b$.

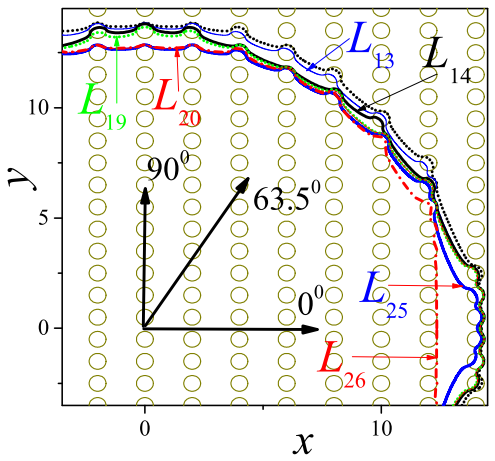

FIG. 7. Parts of the RCLs of a drop on a substrate with $\{\theta^d = 30^\circ,\ \theta^b = 80^\circ\}$ at defect surface concentration $p = 0.2$ on a rectangular lattice of defects with periods $\lambda_1 = 2$, $\lambda_2 = 1$. CLs L_{25}, L_{13}, and L_{19} are the CLs just before the depinning in directions $\varphi = 0^\circ$, 63.5°, and 90°, respectively; CLs L_{26}, L_{14}, and L_{20} are the respective CLs after the depinning.

This is understandable, given that in this depinning regime the elastic force overcomes the pinning force at the center of the part of the CL located on one row of defects (as shown in Fig. 3). The ends of this part of the CL introduce a small correction to the total elastic force acting at the central portion of this part of the CL. Therefore, this depinning regime is an approximation of the situation of an infinite CL located on a single line of defects, and this is the basic assumption of the block depinning model leading to Eq. (4). Taking into account that $\theta^d > \theta^b$, one has $\theta_0^{\max} > \theta_{45}^{\max}$, and therefore in this case the ACA equals $\theta_0^{\max}$.

The analysis of the relationship between the numerically obtained CL depinning and the ACA for a drop on a square grid of defects shows that the biggest CA depends on the linear fraction of defects along a direction perpendicular to the direction of the CL motion. Therefore, one can deduce that the ACA is defined by the row of defects with highest linear fraction. The numerical studies confirm that these results are valid even if the defects are located on a rectangular grid.

RCA. The analysis of the obtained numerical results for a square lattice show that the results for the smallest CAs, $\theta_0^{\min}$ and $\theta_{45}^{\min}$, for CL motion along directions 0° and 45° as a function of the defect concentration p significantly deviate from the predictions of the RCA $\bar{\theta}^r$ of the block depinning model; in the last one for the RCA $\bar{\theta}^r$ one has the following relations:

$$\cos\bar{\theta}^r = p_l \cos\theta^d + (1 - p_l)\cos\theta^b \text{ when } \theta^d < \theta^b, \quad (6)$$

$$\bar{\theta}^r = \theta^b \text{ when } \theta^d > \theta^b. \quad (7)$$

The reason for this is the essential role of the substrate region, in which the CL passes from one row of defects to another row in the process of CL depinning. The difference for the smallest CAs, obtained numerically in both types of CL kink depinning regimes from the predictions of Eqs. (6) and (7), can be seen in Fig. 6. The numerical results for the smallest CAs, $\theta_0^{\min}$ and $\theta_{45}^{\min}$, are shown by circles (solid circles in direction 0° and empty in direction 45°) and a thin (black) line for $\theta^d < \theta^b$, and by squares (solid squares in direction 0° and empty in direction 45°) and a bold (black) line for $\theta^d > \theta^b$. The results for $\bar{\theta}^r$ [Eqs. (6) and (7)] are represented by dashed (red) lines, thin for $\theta^d < \theta^b$ and bold for $\theta^d > \theta^b$, respectively. In Fig. 6 Cassie's angles θ^C [Eq. (2)] are also shown by dash-dotted (blue) lines—thin for $\theta^d < \theta^b$ and bold for $\theta^d > \theta^b$. As expected, it can be seen that as a result of the kink depinning, the smallest CAs along both studied directions, 0° and 45°, of CL displacements are closer to Cassie's angle than to the value for the RCAs $\bar{\theta}^r$ from Eqs. (6) and (7), following from the block depinning model. The deviations of the numerically obtained smallest CAs for liquid drop, $\theta_0^{\min}$ and $\theta_{45}^{\min}$, from $\bar{\theta}^r$ as a function of p are different when $\theta^d < \theta^b$ and when $\theta^d > \theta^b$. In the case when the KD-type depinning for a drop is triggered by a detachment from a defect ($\theta^d < \theta^b$), as can be seen from Fig. 6, the smallest CAs $\theta_0^{\min}$ and $\theta_{45}^{\min}$ along both directions of CL displacement deviate from the predictions for the RCA of the block depinning model $\bar{\theta}^r$ [Eq. (6)] for all defect concentrations studied, i.e., for $0.1 \leqslant p \leqslant 0.55$. The deviation is significant and depends to a certain degree on the concentration. In the studied interval $0.1 \leqslant p \leqslant 0.55$, $\theta_{45}^{\min}$ is slightly bigger than $\theta_0^{\min}$; the difference between them practically does not depend on the defect concentration. Thus in this case one gets that the RCA is $\theta_0^{\min}$.

The RCA in the case where the centers of defects are located on a rectangular grid with $\lambda_1 > \lambda_2$ is the smallest angle among the minimal CAs determined along the directions 0°, $\tan^{-1}(\lambda_2/\lambda_1)$, and 90°. The numerical studies indicate that the smallest CAs in directions 0°, 90° are equal and depend only on the defect surface concentration p (but not on the ratio λ_1/λ_2). The obtained results for the CL displacements on a rectangular lattice of defects is shown in Fig. 7 at defect concentration $p = 0.2$. The defect radius is the same as in Fig. 4 (at $p = 0.4$ and square defect lattice), but the distance between the defects centers along the x axis is doubled ($\lambda_1 = 2\lambda_2$). The CLs preceding the depinning and the CLs after the depinning along directions 0°, $\tan^{-1}(\lambda_2/\lambda_1)$, 90° in Fig. 7 are L_{25}, L_{26}; L_{13}, L_{14}; L_{19}, L_{20}, respectively. The resulting smallest CAs along directions 0°, 90° are identical, and the obtained value

is approximately equal to the value of $\theta_0^{\min}$ in the case of a square grid of defects at defect concentration $p = 0.2$ (shown in Fig. 6). The smallest CA along direction $\tan^{-1}(\lambda_2/\lambda_1)$ is significantly bigger. Therefore, the RCA is equal to $\theta_0^{\min} \equiv \theta_{90}^{\min}$, from which it follows that the RCA depends on the surface defect concentration p but it is not a single-valued function of the linear defect fraction, as predicted by the block depinning model. This result was experimentally established in Ref. [15] for drops on hydrophobic surfaces. In the case when the kink depinning is initiated by a contact with a new defect ($\theta^d > \theta^b$) (KR-type depinning), the transition of the CL to a new row of defects is preceded by detachment of the part of the CL from the outer row of defects. As a result, long sections of the CL appear to be located solely on the homogeneous base Σ_s^b. As the surface defect concentration decreases, the size of these sections increases and there the CL converges towards a circular shape. Therefore, for small defect concentrations ($p \leqslant 0.2$) at the bigger part of the CL in this area, the local CA is equal to θ^b, and at the small parts of the CL touching the defects, it is very close to it. This leads to an apparent CA also close to θ^b, as predicted for the RCA $\bar{\theta}^r$ by the block depinning model. At higher defect concentrations [e.g., at $p = 0.4$, see Fig. 5(b)] along the 0° direction the CL before depinning is in contact with larger parts of the defects in the outermost row, resulting in both a more wrinkled drop interface and greater deviation of the local CA from θ^b at these parts of the CL. By increasing the radius of the defects (at a fixed distance between their centers), i.e., as p increases, the CL more quickly touches a defect from the inner row, leading to a cascading series of depinnings from single defects. As a result, the shape of this CL is more wrinkled, resulting in a greater deviation of the smallest CAs $\theta_0^{\min}$, $\theta_{45}^{\min}$ from θ^b, which is the RCA $\bar{\theta}^r$ of the block depinning model. The results in Fig. 6 show that for $p > 0.2$, $\cos\theta_0^{\min}$, $\cos\theta_{45}^{\min}$ as a function of p deviate from $\cos\theta^b$, with the differences rapidly increasing with p; however, the deviation of $\cos\theta_{45}^{\min}$ is considerably larger than that of $\cos\theta_0^{\min}$. Therefore the RCA is $\theta_0^{\min}$. The numerical studies for a *rectangular grid* of defects with $\lambda_1 > \lambda_2$, $\lambda_1 \leqslant 3$ point once again (as in the preceding case of $\theta^d < \theta^b$) to the dependence of the RCA on the surface concentration p.

B. Hydrophobic surfaces

For the study of hydrophobic surfaces, as a representative case we choose first the values of $180° - 30°$ and $180° - 80°$ for the pair of angles $\{\theta^d,\ \theta^b\}$, since for the hydrophilic surface we have chosen 30° and 80° for the pair $\{\theta^d,\ \theta^b\}$. Here again we perform a numerical study of the drop shape evolution for both cases when $\theta^d < \theta^b$ and $\theta^d > \theta^b$. Analysis of the obtained results for these hydrophobic surfaces shows that they are related to the results for the CL state evolution and the CAH on hydrophilic surfaces, characterized by CAs 30° and 80°. We named the obtained relations between the results for hydrophilic and hydrophobic surfaces principles of "corresponding lines" and "complementary angles," respectively.

1. Corresponding lines and complementary angles

The principle of "corresponding lines" finds expression in the fact that for every equilibrium CL of a drop resting on a substrate, characterized by CAs $\{\theta^d,\ \theta^b\}$, there exists an equilibrium drop resting on a substrate having the same defect pattern, but characterized by CAs $\{180° - \theta^b,\ 180° - \theta^d\}$, and which has the same CL. The sum of the apparent contact angles of both drops at every point of the CL is 180°. We call this property the principle of "complementary angles." In the context of the study of hydrophobic surfaces, these principles manifest themselves in the fact that at the start of the numerical investigation, with a spherical cap approximation with circular CL having radius $R = 14$, on a substrate characterized by CAs $\{180° - \theta^b,\ 180° - \theta^d\}$ the sequence of CLs generated by drop volume increase (decrease) coincides with that obtained for a drop volume increase (decrease) on a hydrophilic surface characterized by CAs $\{\theta^d,\ \theta^b\}$ (the case studied above in Sec. III A). In particular, for these cases the initial CLs L_0, the CLs immediately preceding the depinning (in a given direction of a CL motion), and the CLs appearing after the depinning coincide with each other. In addition to that, the two equilibrium drops with one and the same CL form at every point of the CL apparent CAs whose sum is 180°. To illustrate the principle of complementary angles in Fig. 8, quarters (in 3D subspace $x \geqslant 0,\ y \geqslant 0$) of the two drops resting on hydrophilic and hydrophobic surfaces are represented in the regions $z \geqslant 0$ and $z \leqslant 0$, respectively. The hydrophilic solid substrate is characterized by CAs $\{\theta^d = 30°,\ \theta^b = 80°\}$ and $p = 0.4$. For this case the CL L_{27}, resulting from the depinning of the CL along direction 0°, is shown previously in Fig. 4. It can be seen that the two drop shapes form a continuous surface and the union of the two surfaces is very close to a sphere, but having a deformation in the vicinity of the $z = 0$ plane. In Fig. 8(b) a blown-up image is presented of the result shown in Fig. 8(a), in the vicinity of the area where the CL depinning occurs. The dashed (red) line shows the fitting line of the free drop surface (some distance

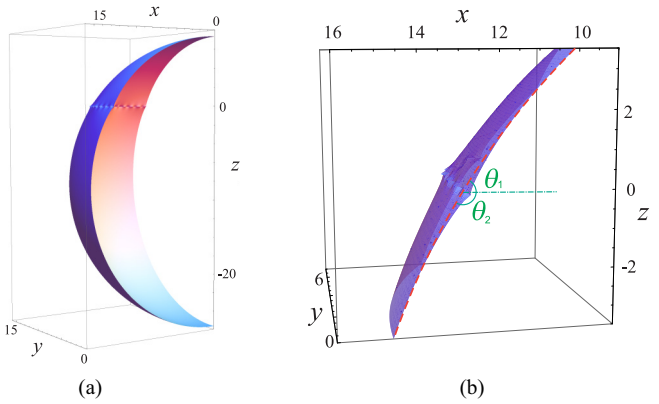

FIG. 8. (a) Parts (in 3D subspace $\{x \geqslant 0, y \geqslant 0\}$) of the two free drop shapes on solid substrates, characterized by CAs $\{\theta^d = 30°,\ \theta^b = 80°\}$ ($z \geqslant 0$) and CAs $\{180° - \theta^b,\ 180° - \theta^d\}$ ($z \leqslant 0$), respectively. The defect surface concentration is $p = 0.4$. Both drops share a common CL, L_{27}, resulting from the depinning of the CL along direction 0°, shown previously in Fig. 4. (b) A blown-up image of the result shown in (a), in the vicinity of the common CL. The dashed (red) line shows the fitting line of the free drop surface (some distance away from the CL) in the plane $y = 0$, used to determine the apparent CA.

away from the CL) in the plane $y = 0$, used to determine the apparent CA. One can see that the sum of the apparent CAs θ_1 (in the case $\{\theta^d = 30^\circ,\ \theta^b = 80^\circ\}$) and θ_2 (in the case $\{\theta^d = 100^\circ,\ \theta^b = 150^\circ\}$) is indeed 180°.

2. Depinning regimes and CAH

The principles of corresponding lines and complementary angles allows one to use the results obtained for the drop CL depinning regimes and the CAH, results from Sec. III A for a drop on hydrophilic surfaces, and apply them to the drop resting on hydrophobic surfaces.

The CL depinning in the advancing regime (Figs. 2 and 3) also represents the depinning of the drop ACL on substrates with CAs $\{\theta^d = 100^\circ,\ \theta^b = 150^\circ\}$ and $\{\theta^d = 150^\circ,\ \theta^b = 100^\circ\}$, respectively. Similarly, Figs. 4 and 5 describe the depinning of the drop RCL on $\{\theta^d = 100^\circ,\ \theta^b = 150^\circ\}$ and on $\{\theta^d = 150^\circ,\ \theta^b = 100^\circ\}$ substrates. Therefore, for hydrophobic surfaces the ACA is again well described by the predictions obtained in Ref. [12] (under the assumption that the whole CL is positioned on one row of defects). Thus, when $\theta^d < \theta^b$ – the ACA equals θ^b, and when $\theta^d > \theta^b$ the ACA is given by the linearized Cassie equation [7].

The values of the drop ACA on $\{\theta^d = 100^\circ,\ \theta^b = 150^\circ\}$ and on $\{\theta^d = 150^\circ,\ \theta^b = 100^\circ\}$ substrates are determined from Eqs. (3) and (7), respectively. The values of the smallest CAs in directions 0°, 45° on the hydrophobic surfaces $\{\theta^d = 100^\circ,\ \theta^b = 150^\circ\}$ and $\{\theta^d = 150^\circ,\ \theta^b = 100^\circ\}$ are calculated from the results shown in Fig. 6 for the smallest CAs in directions 0°, 45° on the hydrophilic surfaces $\{\theta^d = 30^\circ,\ \theta^b = 80^\circ\}$ and $\{\theta^d = 80^\circ,\ \theta^b = 30^\circ\}$, respectively. The following relation holds for the above studied hydrophobic and hydrophilic surfaces:

$$\cos\left(\theta_0^{\min};\ \theta_{45}^{\min}\right)|_{\text{hydrophobic surface}} = \cos\left(\theta_0^{\min};\ \theta_{45}^{\min}\right)|_{\text{hydrophilic surface}} - 1. \quad (8)$$

For hydrophobic surfaces, the RCA is bigger than the prediction of the block depinning model, according to which when $\theta^d < \theta^b$ the RCA is described by the linearized Cassie equation, and when $\theta^d > \theta^b$ the RCA equals θ^b. The deviations of the RCA from the predictions of the block depinning model depend on the defect concentration p, and they are different functions of p in the two cases $\theta^d > \theta^b$ and $\theta^d < \theta^b$. The type of deviation is illustrated well by the results shown in Fig. 6. For an exhaustive numerical study of the RCA, one needs to perform a three-parametric study of the RCA as a function of θ^d, θ^b, and p, and this is beyond the scope of the present work. Here, we limit our studies to the case where for one of the phases the equilibrium CA is 180°. For the CA of the other phase we will use values which are found in the experiments.

3. Physical defects

The analysis of the depinning regimes and the magnitude of the CAH for a drop on smooth and chemically heterogeneous surfaces, as mentioned in the Introduction, is also applicable to rough surfaces with pillars or with holes when a liquid drop contacts the substrate in the Cassie-Baxter wetting regime. If the angle θ^b, characteristic for the homogeneous base, is increased to $\theta^b = 180^\circ$, then the resulting heterogeneous surface describes the behavior of a drop on a surface with pillars (having circular cross-section) in the place of the chemical defects. If the defect-specific angle θ^d is increased to $\theta^d = 180^\circ$, then one can study the behavior of a drop on a surface with holes at the defect location.

Thus we find that the start of the ACL depinning on a surface with pillars (Fig. 2) and of the RCL depinning on a surface with holes (Fig. 5) is initiated by reaching a defect from a neighboring row. This realization of depinning is accompanied by a quick transition of the CL through the new defect whose border it has reached and is also accompanied by a detachment of a big part of the CL from the previous row of defects, and this part remains positioned between the rows of defects. The start of the RCL depinning on a surface with pillars (Fig. 4) and of the ACL depinning on a surface with holes (Fig. 3) is initiated by detachment of the CL from a defect. The CL detachment is not accompanied by a transition of the CL through the whole surface of a new defect. These kinds of identifying characteristics of the depinnings are observed experimentally in Ref. [14] (see movies 1, 4, and 2, 3, respectively, in the Supplemental Information).

For both types of rough surfaces, we find that the depinning is the block case in the advancing regime, and the ACA is described by Eqs. (3) and (5), correspondingly. In the receding regime, we find that the depinning is kink case; however, the values of the RCA are not well described by the results of the block case model of depinning. The RCA as a function of the pillar or hole surface concentration has the behavior displayed in Fig. 6.

In order to verify these results, the RCL and RCA on two particular realizations of the rough surface were investigated numerically for the case where the second angle of the heterogeneous surface is 90° (this angle characterizes the contact with the surface on the top of the cylindrical pillars in the experimental studies by Gauthier *et al.* [18]).

Pillars. Our numerical simulations confirm the experimental results of Gauthier *et al.* [18], indicating that for a drop in the receding mode there is a kink depinning regime when the CL moves along the 0° direction. Figure 9(a) presents our numerical simulation results for the CL depinning for a drop on the surface studied experimentally in Ref. [18] at defect surface concentration $p = 0.2$. The notations in the figure are the same as in Figs. 2–5. A part of the numerically obtained 3D equilibrium drop shape with a contact line L_{127}, just before the depinning of the CL in direction 0°, is shown in Fig. 9(b) in the vicinity of the area where the CL depinning occurs. The enlarged view allows one to see the triangulation mesh used to approximate the drop interface in the numerical minimization algorithm. For this substrate the RCA is determined. One can clearly observe that Fig. 9(a) is very similar to Fig. 4(a). The depinning and the transition of the CL L_{127} to L_{128} is realized in the same way as that shown in Fig. 4(b) and observed experimentally by Gauthier *et al.* [18]. Numerical studies showed that the values of the RCA are in very good agreement with the experimental data shown in Fig. 2 in Ref. [18] and in Fig. 3 in Ref. [15] for pillar concentrations $p \leqslant 0.2$ considered there. For example, at defect surface concentration $p = 0.2$, the experimentally

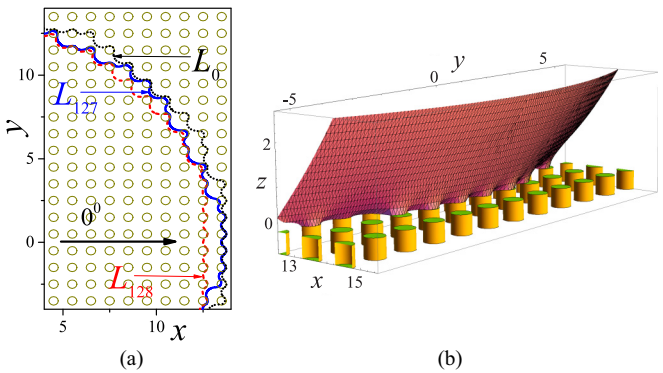

FIG. 9. (a) Parts of the numerically obtained RCLs of a drop on an ultrahydrophobic pillar surface, characterized by CAs $\{\theta^d = 90°, \theta^b = 180°\}$. CL L_{127} is the CL before the depinning, and CL L_{128} is the CL after the depinning. (b) Enlarged view of the 3D equilibrium drop shape with CL L_{127} [shown in part (a)] just before the CL depinning occurs. The triangulation net used to approximate the drop interface is also shown.

established RCA is 126.0°, while the numerical studies for a square lattice of pillars give $\theta^r = 126.2°$. They convincingly show that the RCA is not described by the predictions of the block depinning model. The numerical results strongly support the Barthel group's experimental data that RCA is the result of a kink CL depinning, and its magnitude is much larger than the predictions of the block depinning model. The difference is practically the same as that shown in Fig. 6. In Ref. [5] a formula was suggested for the size of the RCA as a function of the parameters of the solid surface by fitting experimental data, but without any theoretical argumentation. The formula proposed in Ref. [20] by use of the differential area method for doubly periodic defects lattice does not lead to efficient prediction of the contact angles, as pointed out by Gauthier *et al.* [18]. A challenge for further studies would be to obtain such a dependence for both a pillar surface where the RCA should be a function only of p and θ^d, and also for a surface for which $\theta^b < 180°$.

Holes. In this case, the numerical studies show that in the advancing and receding regime the CL depinnings are similar to those shown in Figs. 3 and 5, respectively. The results obtained for the RCA indicate that, at surface defect concentration $p \geqslant 0.2$, its magnitude is not described well by the block depinning model, according to which the RCA is a constant equal to θ^b. The deviation from θ^b has the form shown in Fig. 6 when $\theta^d > \theta^b$, i.e., the numerical simulations predict that the CAH for a drop on a substrate with holes is also smaller than that obtained within the block depinning model at high surface concentrations. Therefore, in this case it has to be modeled through the described specificity of the kink depinning of the CL. The available experimental data for the RCA of a drop on such a substrate as a function of the hole surface concentration are presented in Fig. 4(a) in Ref. [35], in Table 1 in Ref. [36], and in Fig. 2 in Ref. [14]. In Ref. [35] one can detect a trend of RCA increasing with the hole concentration; however, the scatter of data is too large in order to reliably confirm the RCA dependence on the hole concentration. The results in Ref. [36] show increasing RCA with hole concentration, as predicted by our results displayed in Fig. 6, while the results for the RCA in Ref. [14] do not imply dependence on the hole concentration. The experimental data seem to point to a tendency of RCA increasing with the hole concentration, but the data are insufficient for a convincing support of the numerical results. Further experimental investigation of this case is necessary at high hole concentrations. As in the case of pillars, obtaining an analytical dependence of the RCA on the surface parameters is highly desirable.

IV. CONCLUSION

A precise numerical study of the evolution of an equilibrium liquid droplet in contact with doubly periodic microtextured surfaces under drop volume change is performed. The process of stick, slip, and jump motion of the CL is analyzed in detail. Four universal types of depinning regimes are identified, and the distinction is based on the region of the CL where the process starts (i.e., from regions where the equilibrium CL crosses from one row of defects to the next row or from the middle section of the CL, positioned on one row of defects) and on what triggers the start of the depinning (i.e., the CL reaching the border of a defect, belonging to a new row of defects, or the CL detaching from the inner part of a defect).

It is shown that in the case of ACL, the depinning process always starts from the middle section of the CL, positioned on one row of defects, and in the case of a RCL the depinning process starts from the part of the CL where the CL crosses from one row of defects to the next row. It is found that the cause that triggers the depinning process (i.e., the CL reaching or detaching from a defect) is altered by changing the direction of motion of the CL and also by changing the surface tensions of the materials, which form the heterogeneous solid surface. The more detailed study of the CL depinning made it possible to distinguish the existence of different depinning mechanisms, determining the magnitude of the ACA and RCA, and their dependence on the surface and linear fractions of defects. It also gave an answer to which projection of the drop interface, relative to the defect lattice, should be used in the experiments to determine these two angles. Also, a relationship between the results for the CL, ACA, and RCA evolution on hydrophilic and hydrophobic surfaces is established.

The results of our numerical simulations study of the RCL of a liquid drop on a surface with pillars supports the experimental results of Gauthier *et al.* [18] that the transition of the CL to an inner defect row is realized by kink depinning and, accordingly, the RCA value is different from the predictions of the block depinning model. As our studies show, this also holds true for surfaces with holes. The analysis of the results for the ACA and RCA shows that ACA is always well described by the existing predictions, given by Eqs. (3) and (4), which are based on the assumption of block depinning of the CL, located entirely on one row of defects. As for the RCA, finding an analytical expression for the RCA in terms of the surface parameters requires the development of new approximations that determine the overcoming of the stick force by the elastic force in the vicinity of a kink. The obtained

results renew the question of whether it is possible to further decrease the CAH for a drop on heterogeneous surfaces (or rough surfaces with pillars or holes) by varying the design of the defect pattern as well as the size and shape of the defects.

[1] D. Quéré, Annu. Rev. Mater. Res. **38**, 71 (2008).
[2] D. Bonn, J. Eggers, J. Indekeu, J. Meunier, and E. Rolley, Rev. Mod. Phys. **81**, 739 (2009).
[3] H. Y. Erbil, Surf. Sci. Rep. **69**, 325 (2014).
[4] C. Dorrer and J. Rühe, Langmuir **23**, 3179 (2007).
[5] S. Iliev and N. Pesheva, Phys. Rev. E **93**, 062801 (2016).
[6] J. F. Joanny and P. G. de Gennes, J. Chem. Phys. **81**, 552 (1984).
[7] C. Extrand, Langmuir **18**, 7991 (2002).
[8] T. Cubaud and M. M. Fermigier, J. Colloid Interface Sci. **269**, 171 (2004).
[9] C. Priest, R. Sedev, and J. Ralston, Phys. Rev. Lett. **99**, 026103 (2007).
[10] S. T. Larsen and R. Taboryski, Langmuir **25**, 1282 (2009).
[11] M. Reyssat and D. Quéré, J. Phys. Chem. B **113**, 3906 (2009).
[12] R. Raj, R. Enright, Y. Zhu, S. Adera, and E. N. Wang, Langmuir **28**, 15777 (2012).
[13] S. Iliev, N. Pesheva, and V. S. Nikolayev, Phys. Rev. E **90**, 012406 (2014).
[14] Y. Jiang, W. Xu, M. A. Sarshar, and C.-H. Choi, J. Colloid Interface Sci. **552**, 359 (2019).
[15] M. Rivetti, J. Teisseire, and E. Barthel, Phys. Rev. Lett. **115**, 016101 (2015).
[16] L. W. Schwartz and S. Garoff, Langmuir **1**, 219 (1985).
[17] C. Dorrer and J. Rühe, Langmuir **22**, 7652 (2006).
[18] A. Gauthier, M. Rivetti, J. Teisseire, and E. Barthel, Phys. Rev. Lett. **110**, 046101 (2013).
[19] T. Cubaud and M. Fermigier, Europhys. Lett. **55**, 239 (2001).
[20] W. Choi, A. Tuteja, J. Mabry, R. Cohen, and G. McKinley, J. Colloid Interface Sci. **339**, 208 (2009).
[21] H. Kusumaatmaja and J. M. Yeomans, Langmuir **23**, 6019 (2007).
[22] N. Anantharaju, M. V. Panchagnula, and S. Vedantam, Langmuir **25**, 7410 (2009).
[23] S. Iliev and N. Pesheva, J. Colloid Interface Sci. **301**, 677 (2006).
[24] A. Marmur, C. Della Volpe, S. Siboni, A. Amirfazli, and J. Drelich, Surf. Innovations **5**, 3 (2017).
[25] A. F. Stalder, G. Kulik, D. Sage, L. Barbieri, and P. Hoffmann, Colloids Surf. A **286**, 92 (2006).
[26] J. A. Marsh and A. M. Cazabat, Phys. Rev. Lett. **71**, 2433 (1993).
[27] D. Iliev, N. Pesheva, and S. Iliev, Langmuir **29**, 5781 (2013).
[28] S. Iliev, Comput. Methods Appl. Mech. Engrg. **126**, 251 (1995).
[29] K. Brakke, Exp. Math. **1**, 141 (1992).
[30] S. Iliev and N. Pesheva, Langmuir **19**, 9923 (2003).
[31] S. Iliev, N. Pesheva, and V. S. Nikolayev, Phys. Rev. E **72**, 011606 (2005).
[32] P. G. de Gennes, Rev. Mod. Phys. **57**, 827 (1985).
[33] T. Blake, J. Colloid Interface Sci. **299**, 1 (2006).
[34] C. W. Extrand, Langmuir **32**, 8608 (2016).
[35] C. Priest, T. W. J. Albrecht, R. Sedev, and J. Ralston, Langmuir **25**, 5655 (2009).
[36] M. Kanungo, S. Mettu, and K.-Y. Law, Langmuir **30**, 7358 (2014).